Queen's University
Belfast

Probing charge screening dynamics and electrochemical processes at the solid–liquid interface with electrochemical force microscopy

Published in:
Nature Communications

Document Version:
Peer reviewed version

Queen's University Belfast - Research Portal:
Link to publication record in Queen's University Belfast Research Portal

Publisher rights

General rights

Take down policy

Probing charge screening dynamics and electrochemical processes at the solid-liquid interface with electrochemical force microscopy

Liam Collins,[1,2] Stephen Jesse,[3] Jason I. Kilpatrick,[2] Alexander Tselev,[3] Olexander Varenyk,[4] M. Baris Okatan,[3] Stefan A. L. Weber,[2] Amit Kumar,[3] Nina Balke,[3] Sergei V. Kalinin[3] & Brian J. Rodriguez[1,2]

[1]School of Physics, University College Dublin, Belfield, Dublin 4, Ireland

[2]Conway Institute of Biomolecular and Biomedical Research, University College Dublin, Belfield, Dublin 4, Ireland

[3]Center for Nanophase Materials Sciences, Oak Ridge National Laboratory, Oak Ridge, Tennessee 37831, USA

[4]Taras Shevchenko Kiev National University, Radiophysical Faculty, 4g, pr. Akademika Hlushkova, 03022 Kiev, Ukraine

The presence of mobile ions complicates the implementation of voltage modulated scanning probe microscopy techniques such as Kelvin probe force microscopy (KPFM). Overcoming this technical hurdle, however, provides a unique opportunity to probe ion dynamics and electrochemical processes in liquid environments and the possibility to unravel the underlying mechanisms behind important processes at the solid-liquid interface including adsorption, electron transfer, and electrocatalysis. Here, we describe the development and implementation of electrochemical force microscopy (EcFM) to probe local bias- and time-resolved ion dynamics and electrochemical processes at the solid-liquid interface. Using EcFM, we demonstrate contact potential difference measurements, consistent with the principles of open loop KPFM operation. We also demonstrate that EcFM can be used to investigate charge screening mechanisms and electrochemical reactions in the probe-sample junction. We further establish EcFM as a force-based imaging mode, allowing visualization of the spatial variability of sample-dependent local electrochemical properties.

Correspondence should be addressed to B.J. Rodriguez (email: brian.rodriguez@ucd.ie).

Understanding local electrostatic and electrochemical phenomena at the solid-liquid interface is crucial to areas ranging from corrosion,[1,2] sensing,[3] energy conversion[4] and storage[4,5] to biology and biochemistry.[6] Of particular interest are the local electrochemical processes governing the operation of energy conversion and storage devices, such as lithium ion batteries,[7] electrochemical capacitors,[8] and fuel cells.[9] Significant progress has been achieved in developing a theoretical understanding of the complex diffuse charge dynamics in electrochemical systems, involving both Faradaic (e.g., redox reaction) and non-Faradaic (e.g., electric double layer charging) processes.[10-13] However, a complete understanding of such processes requires scanning probe microscopy (SPM) techniques capable of mapping electrostatic and electrochemical phenomena at the solid-liquid interface with a lateral resolution commensurate with the length scale of the phenomena.

In ambient and vacuum environments, the electrostatic properties of surfaces can be mapped by Kelvin probe force microscopy (KPFM).[14-16] In KPFM, the electrostatic force, $F_{el} = -\frac{1}{2}C'_z(V_{tip}-V_{cpd})^2$, acting on a probe due to the application of a tip voltage, $V_{tip} = V_{dc} + V_{ac}\sin(\omega t)$, is detected via the first harmonic electrostatic force response of the cantilever, $F_{\omega} = -C'_z(V_{dc}-V_{cpd})V_{ac}\sin(\omega t)$, where V_{ac} and V_{dc} are AC voltage and DC bias applied to the tip (or sample), C'_z is the tip-sample capacitance gradient, and V_{cpd} is the contact potential difference (CPD).[14] A feedback loop is employed to minimize the first harmonic response through the application of a DC bias proportional to the CPD between the probe and sample. The second harmonic component of the electrostatic force, $F_{2\omega} = \frac{1}{4}C'_z V_{ac}^2\cos(2\omega t)$ is assumed to be independent of the CPD and DC bias. In order to obtain meaningful materials and system properties using conventional KPFM, the dielectric in the tip-sample junction must behave like a lossless dielectric (e.g., a vacuum), resulting in both a first harmonic response that is linear with

2

respect to applied DC bias and a time-invariant electrostatic force. At the same time, the measurement itself must not alter the true CPD.

These conditions, fundamental to conventional KPFM operation, are expected to be violated in liquids containing mobile ions when AC voltage and/or DC biases are applied due to bias-induced electrochemical and electrokinetic phenomena.[17,18,19] To date, KPFM has been implemented in liquid in the absence of ions (non-polar liquid)[20] and limited progress has been obtained in low molarity electrolytes (< 10 mM) using KPFM modes which do not require bias feedback (i.e., open loop KPFM).[21,22] Whilst, electrostatic forces are increasingly being used to actuate atomic force microscope (AFM) cantilever motion in liquids in order to measure surface topography,[23-26] surface charge density,[26] and dielectric constants,[27-29] voltage modulated (VM)-SPM imaging in conductive electrolytes presents an unresolved challenge.

Indeed, in the presence of mobile ions, AC voltage and/or DC bias applied between tip and sample are expected to result in bias-induced charge dynamics, ion diffusion, and ultimately Faradaic reactions. These processes alter the force experienced by a VM-SPM probe, precluding meaningful materials and system properties from being obtained using KPFM in the presence of ions, and necessitating the development of a suitable technique to study their influence systematically. Here, we establish such a technique, paving the way for quantitative, force-based electrochemical measurements in liquid. First, we describe the role mobile ions have on VM-SPM measurements in liquids by modelling the time-dependent ion dynamics for the simplified case of a 1D parallel plate capacitor.[30,31] We then develop and implement a multidimensional, bias- and time-resolved spectroscopic approach, referred to as electrochemical force microscopy (EcFM). We demonstrate the capability of EcFM to determine CPD under specific conditions and to probe charge screening mechanisms and electrochemical reactions in the probe-sample

junction. Finally, we validate EcFM as an imaging mode on a sample with disparate electrochemical properties across its surface.

Results

Charging dynamics

Recent reports of charge density[26] or electric potential[21,22] mapping have been based on the assumption of the presence of a lossless dielectric and hence, a time-invariant electric field in the tip-sample junction. To date, little consideration has been given to the role ion dynamics play on the forces experienced by a VM-SPM probe in liquid. Following the work of refs 10,30,31, we illustrate the influence of diffuse charge dynamics on VM-SPM measurements performed in the presence of ions by considering the simple case of a 1D parallel-plate capacitor with ion-blocking electrodes (i.e., a non-Faradaic system). We numerically solve the time-dependent ion transport equations using COMSOL Multiphysics and adopting a modified Poisson-Nernst-Plank model.[30,31] The model takes into account non-linear phenomena such as ion diffusion and steric effects including ion crowding, which become particularly important at larger biases ($>> kT/e$) and higher ion concentrations. For clarity, we first determine the charge dynamics of the system in response to the application of a small voltage step (30 mV), where steric effects are largely absent (Fig. 1a). The electrodes are separated by a distance $L = 200$ nm in a 10 mM 1:1 electrolyte. We observe a time varying non-linear potential distribution in the electrode junction. The time it takes the system to reach a steady state (~ 50 μs, dashed line in Fig. 1a) can be understood when one considers the relaxation time scales associated with the various electrochemical phenomena involved in reaching electrochemical equilibrium. Once the circuit is closed, ions undergo electromigration in response to the applied electric field, forming electric double layers which electrically screen the polarized electrode. The time it takes an ion to diffuse

4

across the electric double layer is the Debye time, $\tau_D = \lambda^2 / D$, where λ is the Debye screening length and D is the ion diffusivity across λ (ref. 10). The Debye time is typically in the ns – µs range for low molarity aqueous solutions and is 5.2 ns for the model electrolyte capacitor used in Fig. 1a. Even after the formation of the electric double layers, the system has yet to achieve electrochemical equilibrium. The ion concentration gradient away from the electrode surface induces diffusion of ions towards the electrodes, resulting in a net uptake of ions from the neutral bulk electrolyte into the double layer. The timescale of this bulk diffusion process, $\tau_L = (L/2)^2 / D$, where L is the electrode separation, is usually much slower (5.7 µs for Fig. 1a) than the Debye time, as it is governed by the geometry of the system.[10] The third major time scale in the system is the time required for the diffuse layer charge relaxation through bulk electrolyte conduction, $\tau_C = \sqrt{\tau_D \tau_L} = \lambda (L/2)/D$ (172 ns for Fig. 1a). In equivalent circuit theory, this time is referred to as the electric double layer charging time (i.e., RC time, where R and C are the resistance and capacitance of the circuit). These relaxation times are calculated for both milliQ water and 10 mM 1:1 electrolyte in Supplementary Table 1 for capacitors with small (200 nm) and large (15 µm) electrode separations, representing the tip- and cantilever-sample distances employed in this work. For larger biases (> 30 mV), the picture becomes more complicated due to ion crowding and ultimately Faradaic reactions for non-blocking electrodes.

Diffuse charge dynamics are present for all tip-sample and cantilever-sample separations, and need be taken into consideration for all VM-SPM experiments in liquids containing ions. Even under a purely AC voltage excitation, careful consideration must be paid to the timescales of voltage-induced electrochemical processes. Fig. 1b shows the evolution of the concentration-dependent (τ_D, τ_C) and independent (τ_L) time constants as a function of the calculated relaxation times and ion concentration. The red box indicates the frequency space currently

accessible using commercial AFM systems (DC – ~ 10 MHz). Notably, it may be possible to determine the electronic properties (e.g., CPD[32] and dielectric constant[27,28]) of the sample when operating in region III, where the electric double layer charging and ion diffusion processes occur at a time scale much slower than the measurement time (i.e., mobile ions are in quasi-static equilibrium).[32] While measurements of CPD in higher (> 100 mM) ion concentrations are attractive for many energy and biological systems, they become impractical in the presence of ion dynamics (region II) and Faradaic processes at longer time scales (region I). At the same time, operating in regions I and/or II presents an opportunity to probe important electrochemical phenomena in the tip-sample junction. These considerations necessitate the development of a multidimensional spectroscopic approach to investigate the role ion dynamics and electrochemical processes play on the forces experienced by a VM-SPM probe.

Electrochemical force microscopy

The complex time and bias dependence in regions I and II preclude describing ion dynamics in terms of a single parameter (e.g., CPD as determined by conventional KPFM). Hence, probing electrochemical phenomena at the solid-liquid interface requires probing bias- and time-resolved dynamics at each spatial point. Here, we have developed such a multidimensional spectroscopic approach, referred to as EcFM.

In EcFM measurements, the tip is positioned a specified distance (200 nm for measurements shown) from the surface, and electrochemical processes in the tip-sample junction are activated using a set of bipolar pulses (typically 50 – 100 ms) amplitude-modulated by a slowly varying linear waveform (0.01 Hz). A single frequency AC excitation (Fig. 2a) is used with lock-in detection to record both the amplitude and phase of the first (A_ω and θ_ω, respectively) and second (or higher) harmonic response. The EcFM data is collected both during

the bias application (bias-on state) and following the bias application (bias-off state). Here, we consider only the bias-on state. In air, the cantilever rapidly responds to the applied bias and quickly reaches, and remains, at equilibrium (Fig. 2b). The amplitude response in air has a linear bias dependence, verifying a purely electrostatic response and satisfying key requirements for determining the CPD using conventional KPFM. In liquid, the scenario is more complex and several characteristic bias regimes of dissimilar behaviour are present (Fig. 2c). For example, at low biases (< 500 mV) the signal shows a relatively weak bias dependence, with small transient processes becoming visible above 200 mV. At larger biases (> 500 mV), a relatively strong EcFM response is activated initially, followed by subsequent transient relaxation. Note that the observed non-linear bias dependence and transient relaxation of the response violates the key requirements for performing conventional KPFM.

An alternative illustration of a typical first harmonic EcFM amplitude response is shown in Fig. 3a, where a 2D plot represents the bias and time dependence for a single location, recorded in milliQ water 200 nm above an Au electrode. The maximum in the EcFM amplitude response occurs at < ~ 10 ms, relaxing to an equilibrium value within the measurement window (100 ms). Slight divergence from this equilibrium baseline becomes visible at higher biases (> 500 mV). This relatively high response at fast detection rates is comparable to other pulsed electrochemical techniques, where capacitive charging of the electric double layer dominates the response.[33] Similar to KPFM in air, for fast EcFM detection (< 1 ms) in milliQ water, we observe a linear bias dependence and amplitude minimum, suggesting that the EcFM response is dominated by an electrostatic interaction (i.e., Maxwell stress) in this regime. Under such circumstances, EcFM operation is in principle equivalent to open loop KPFM operation.[34] The CPD between the tip and Au electrode at 500 μs was determined from a linear fit of the EcFM

mixed response (i.e., $A_\omega(cos\theta_\omega)$) vs. bias to be 139 ± 23 mV (Fig. 3b). At longer detection times, however, as partial screening of the charge on the electrode occurs, a unique EcFM amplitude minimum is no longer observed, illustrating why the conditions required for conventional KPFM cannot be satisfied in ion containing solutions. (Supplementary Fig. 1). In general, the response was seen to relax to electrochemical equilibrium within 20 ms (Fig. 3c), consistent with the disappearance of the amplitude minimum (Supplementary Fig. 1).

Unlike KPFM, EcFM contains important information pertaining to charge screening mechanisms (see Supplementary Fig. 2 and 3). To demonstrate this, we modelled the charging of polarized capacitor plates separated by 200 nm (tip-sample) and 15 μm (cantilever-sample) in response to a 250 mV bias pulse in milliQ water (Supplementary Fig. 3). Like in any *RC* circuit, the charging/discharging mechanism of a diffusion driven process is expected to show a simple exponential decay. In this case, the modelled data was found to be best described by a double exponential fit (see Supplementary Fig 5), with relaxation times of 1.86 ± 0.01 ms and 10.27 ± 0.02 ms. This is in agreement with the experimental data in response to a 225 mV step bias, which yields relaxation time constants of 1.24 ± 0.04 ms and 6.28 ± 0.21 ms (Supplementary Fig. 4). Note that EcFM data was recorded with bias steps of 75 mV, thus direct comparison with data recorded at 250 mV was not possible. It was also found that for small biases (< 10 mV) the modelled electric double layer at a terminal plate demonstrated an exponentially decaying response, whereas for larger biases (> 100 mV) a double exponent was required to describe the modelled data (Supplementary Fig. 5). The differences observed between low and high biases are likely a consequence of ion depletion close to the diffuse layers after the electric double layer screening has occurred. With stronger depletion, the ion redistribution from the bulk will be more noticeable, which is expected for larger biases. InSupplementary Fig. 5, for all biases

investigated, the initial relaxation had a time constant of 1.75 ± 0.10 ms, close to that predicted analytically (τ_C = 2.0 ms). For larger biases, a second relaxation process having bias-dependent response times of 3.88 ± 0.07 ms (100 mV) and 10.27 ± 0.05 ms (250 mV) is attributed to the diffusion time of ions from the bulk, τ_L = 31.8 ms. The bias-dependent deviation between the observed timescales and those determined analytically is not surprising, as the analytical values do not take into account the magnitude of ion depletion and hence have no bias-dependent terms. The osmotic pressure component in our model, which is an indicator of the diffusive processes taking place in the system, also relaxed faster than the diffusion timescale predicted analytically (τ_L = 31.8 ms).

To explore the dependence of ion concentration on the electrochemical response, EcFM was used to study an Au electrode as a function of K_2SO_4 concentration (Fig. 4). The first harmonic EcFM amplitude response is represented as response vs. bias where each time is represented by a different colour to effectively show the complex bias dependence and subsequent relaxation present within the data. Measurements are performed at 200 nm from the Au surface in milliQ water and 1 mM, 10 mM, and 100 mM K_2SO_4. In both milliQ water (Fig. 4a) and 1mM K_2SO_4 (Fig. 4b) a bias-dependent response with a minima can be observed in the fast response regime, which quickly relaxes as determined by the *RC* time of the circuit, τ_C. In 1mM K_2SO_4, the transient relaxation time was determined in the same fashion as described for Supplementary Fig. 2a to be 391 ± 90 μs and 1.2 ms ± 0.1 ms , both of which are beyond the experimental detection limit (limited by the lock in amplifier time constant, 100 μs). In contrast, for both 10 mM (Fig. 4c) and 100 mM K_2SO_4 (Fig. 4c), no significant transient relaxation of the bias dependence in the chosen window (-375 mV – +250 mV) is observed. The charge screening is expected to occur faster as the concentration increases (2.0 ms for milliQ water and 12.9 μs for

9

10 mM 1:1 electrolyte, which is well below the current detection limit). To effectively probe charge screening dynamics in higher molarity electrolytes, sub-microsecond detection[35] could be incorporated into the EcFM setup. Interestingly, at larger biases in high molarity solutions, we begin to observe a strongly non-linear response. These processes are too slow (> 75 ms) for ion diffusion across the cantilever-sample separation and are attributed to electrochemical reactions taking place at the solid-liquid interfaces. The activation bias of these processes for negative tip bias begins at ~ -500 mV for both 10 mM and 100 mM, however, larger amplitudes are observed for 100 mM. Further ion concentration-dependent processes are observed at positive biases (> 1.1 V) for 100 mM but not for 10 mM solutions. The concentration-dependence of this 'gap' between the apparent onset of bias-dependent processes warrants further investigation and requires differentiation of reversible and non-reversible processes.

Figs. 3 and 4 demonstrate that EcFM can be used to investigate charge screening dynamics and electrochemical processes in the probe-sample junction depending on the regime (bias, time, ion concentration). Furthermore, EcFM can be used both to determine CPD and to provide information on charge screening mechanisms.

EcFM mapping

The EcFM approach allows the 2D bias- and time-dependent spectroscopic response at a single point to be measured (Fig. 2). The natural question is then whether this strategy can be extended to detect material-specific electrochemical properties and ultimately achieve spatially-resolved EcFM imaging, where EcFM response is sampled in a dense spatial grid. Here, we introduce such a spectroscopic imaging approach.

Shown in Fig. 5 is an example of 2D EcFM imaging in milliQ water across Au electrodes deposited on a SiO_2 layer. Here, 2D EcFM bias- and time-dependent spectroscopic response was

recorded at specified locations in a 30 × 30 grid across the electrodes (Fig. 5a), giving rise to a 4D data set (x, y, bias, time). A quantitative and systematic analysis of the spatial variability of the bias and time dependence of the EcFM response requires a complete physical model of the signal formation mechanism. However, the complexity of the response mechanism in EcFM currently precludes the establishment of a suitable physical model, as is the case for many other AFM techniques (e.g., electrochemical strain microscopy). In order to demonstrate the spatial variability present in the data, we have plotted the first and second harmonic EcFM amplitude response recorded 5 ms after the onset of the +1.5 V and -1.5 V bias pulses (Fig. 5c-f). Average cross sections for each image, from the region indicated in Fig. 5a, are shown in Fig. 5b. The observed spatial variation between Au and SiO_2 is present for all biases and times, as shown in Supplementary Movie 1. For both first and second harmonics, the EcFM response shows a bias-polarity dependence for SiO_2. This suggests that the effective carrier density of the SiO_2 surface has changed between the application of positive and negative biases. For Au, the first harmonic EcFM response is polarity-dependent, whereas the second harmonic response for Au is the same for both ±1.5 V. The presence of such spatially-dependent contrast demonstrates that the EcFM signal is localized and dependent on the electrochemical properties of the material below the tip.

Discussion

We have implemented a generalized approach for electrochemical measurements in liquids containing mobile ions, combining the force-sensitivity of AFM with the ability to probe the bias and time dependence of sample-dependent electrochemical dynamics at the probe-sample junction and spatially across boundaries between dissimilar materials. This approach provides a framework to elucidate details of electrochemical processes at the solid-liquid interface. With improvements in detection time-scales, EcFM can potentially be used to record and deconvolve

fast charge dynamics and electric double layer formation processes in high molarity electrolytes. Furthermore, while practical considerations (e.g., data acquisition time vs. system stability) presently render acquisition of higher density EcFM images challenging, the adoption of fast lock in detection and suitable data visualization approaches (e.g., principal component analysis[36]) can make this technique fully viable.

EcFM has the potential to provide fundamental insight into ion charge diffusion and relaxation as a function of tip-sample separation and frequency (AC voltage and DC bias sweeps), and may be combined with measurements of current for direct comparison with conventional electrochemical measurements. EcFM measurements will be useful in the study of local electrochemically-induced changes in charge density due to both ion adsorption/desorption and electron transfer at the solid-liquid interface and other phenomena central to biological and energy research.

Methods

Sample preparation Au-coated borosilicate glass substrates (Arrandee[TM]) were cleaned in isoproponal and ethanol and rinsed in milliQ water prior to use. For the Au/SiO_2 sample, ~ 45 nm of Au was deposited on ~ 5 nm of Ti by evaporation on top of 100 nm of thermal oxide on Si.

EcFM

The EcFM measurements were performed using Asylum Research, MFP-3D or Park Systems Inc., NX10 AFM systems, a LabView/MatLab controller implemented using National Instruments NI-5122 and NI-5412 fast AWG and DAQ cards, and as-received Pt/Ir-coated (Nanosensors, PPP-EFM) cantilevers with a nominal mechanical resonant frequency and spring constant of 75 kHz and 2.8 N/m, respectively. All measurements were performed using two lock

in amplifiers (Stanford research, SR830 and Signal Recovery, 7280). The time constant of the lock in amplifiers was set to 100 µs. Excitation frequencies of 17.8 kHz with an amplitude of 1 V were used for Figs. 2–4. For Fig. 5, the excitation was 19 kHz with an amplitude of 1 V. For Figs. 2 and 5, the DC bias range was ±1.5 V with 50 ms bias-on and off states, and for Figs. 3 and 4, the DC bias range was ±1.5 V with 100 ms bias-on and off states. The tip-sample separation was set to 200 nm following a force-distance curve for all EcFM measurements.

Author contributions

L.C., S.J., J.I.K., S.V.K., and B.J.R. designed the study. L.C. and S.J. developed the EcFM instrumentation. S.J. prepared the samples. L.C. performed the EcFM experiments. L.C., S.J., M.B.O., and A.K. wrote code to analyse the EcFM data. L.C., A.T., and O.V. modelled ion transport. L.C., S.J., J.I.K., A.T., M.B.O., S.A.L.W., N.B., S.V.K., and B.J.R. analysed data and interpreted the results. L.C., J.I.K., A.T., S.V.K., and B.J.R. wrote the paper. All authors commented on the manuscript.
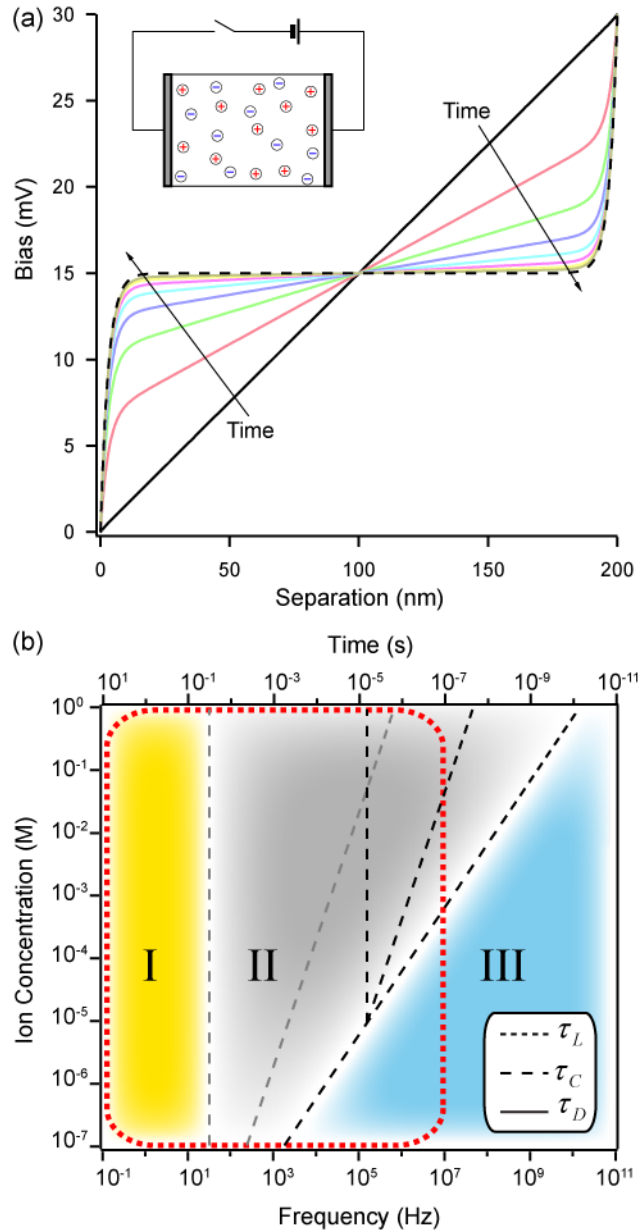
Additional information

Supplementary Information accompanies this paper at

http://www.nature.com/naturecommunications

**Competing financial interests:** The authors declare no competing financial interests.
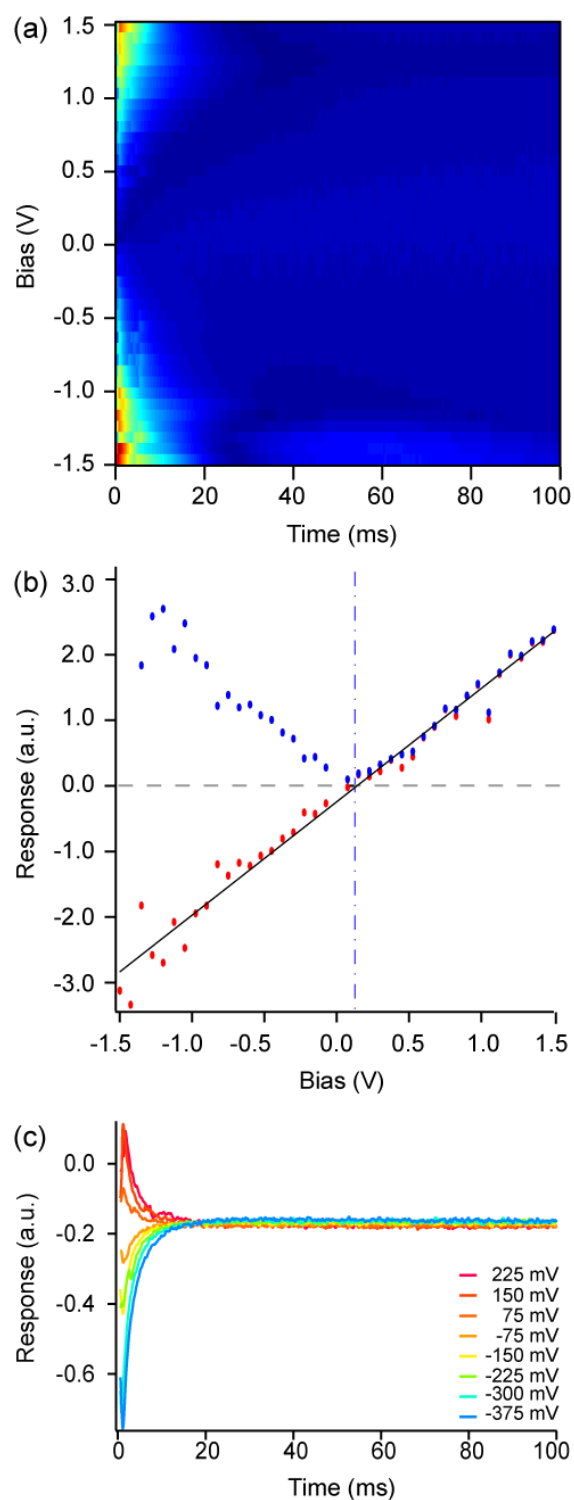
Figures

Figure 1 | Charge dynamics and relaxation processes in the presence of mobile ions. (a) 1D COMSOL model showing the evolution of the bias between plane-parallel electrodes (as shown in the inset) in an 1:1 electrolyte assuming diffusion coefficients, $D_+ = D_- = 1.77 \times 10^{-9}$ m^2/s (corresponding to the Cl$^-$ ion[37]), with an initial concentration of 10 mM in response to application of a 30 mV voltage step applied across the electrodes ($L = 200$ nm). Solid lines show potential distributions at $t = 0$ and then in 100 ns time steps after the bias application. The dashed line shows the distribution at $t = 50$ μs after the bias application, which is indistinguishable from the steady state distribution after the full relaxation of the system. **(b)** The characteristic timescales (Debye time, τ_D, bulk diffusion, τ_L, and charge relaxation, τ_C) as a function of NaCl concentration for 200 nm (black) and 15 μm (grey) electrode separation representing tip- and

15

cantilever-sample, respectively. The region enclosed by the red dashed line indicates the frequency space accessible by AFM. The shaded regions indicate the electrochemical processes expected to be present.
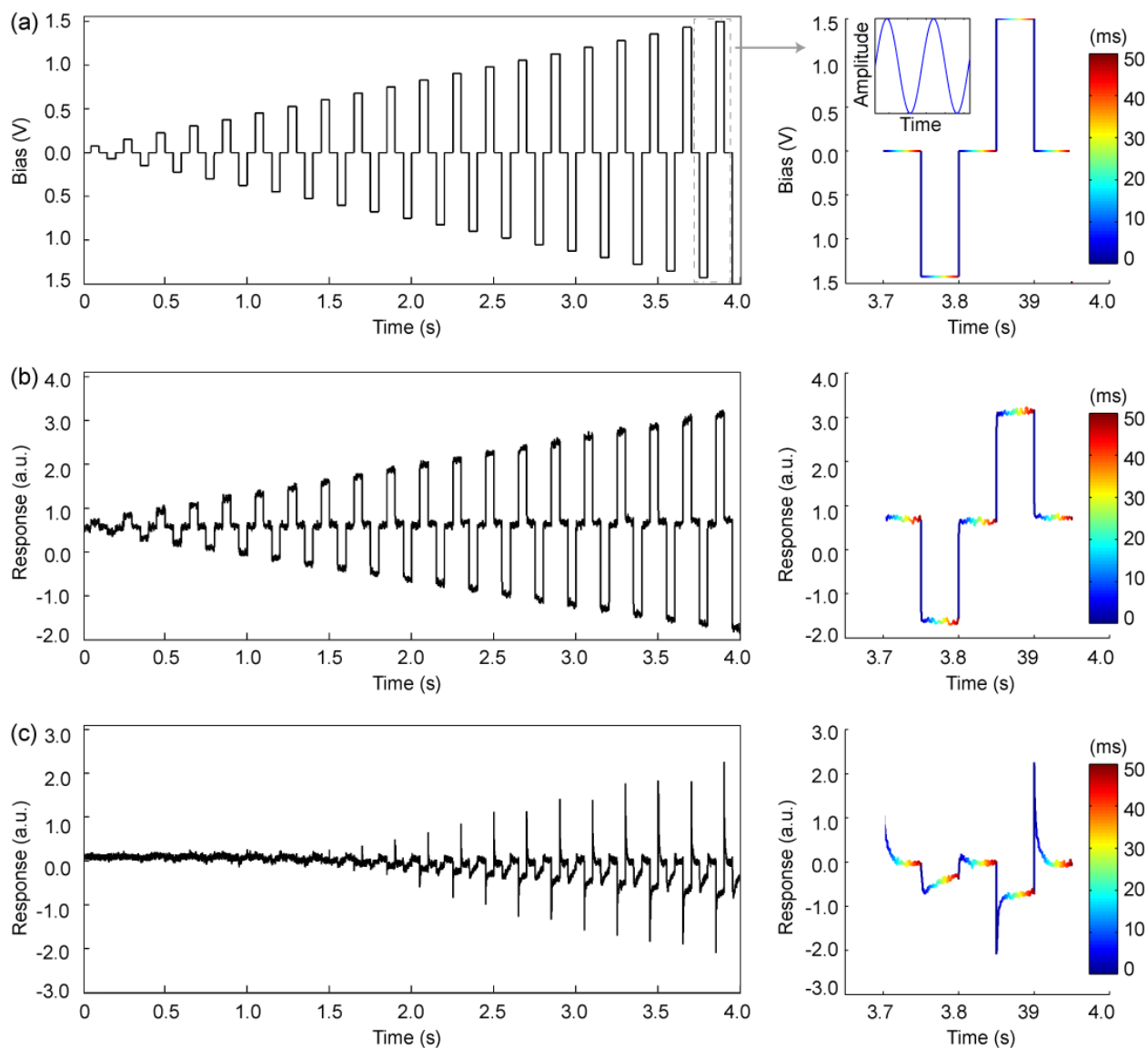

Figure 2 | Electrochemical force microscopy. (a) Waveform applied to the tip in a single point EcFM measurement. A single frequency excitation (inset of **(a)**) is applied to the tip while positive, negative, and zero bias pulses are added to the AC voltage. The EcFM response is recorded during both on and off states (measurement window = 50 ms) to detect excitation and relaxation processes. Shown is the first harmonic mixed response recorded 200 nm above an Au electrode in **(b)** air and **(c)** milliQ water.

Figure 3 | Probing charge screening mechanisms using EcFM. (a) 2D plot of the first harmonic EcFM amplitude response 200 nm above the surface. **(b)** First harmonic EcFM amplitude vs. bias (blue data points) and linear fit (black line) to EcFM mixed response (red data

points) vs. bias dependence for time = 500 μs. The CPD, 139 ± 23 mV, is indicated with dashed blue line. **(c)** EcFM mixed response vs. time for a small bias window (-375 − +225 mV).
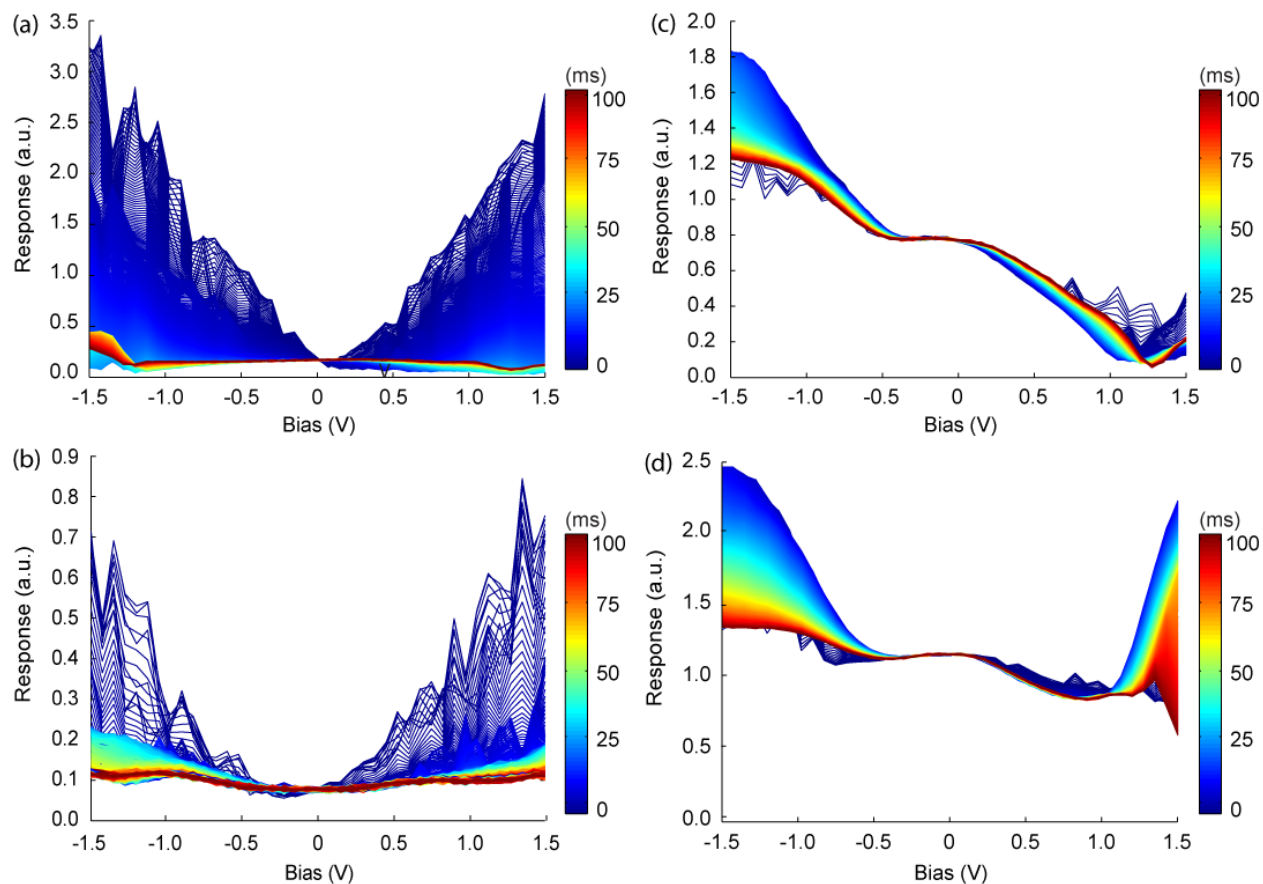
Figure 4 | EcFM data recorded on Au as a function of ion concentration. The first harmonic EcFM amplitude collected 200 nm above an Au electrode in solutions of increasing salt concentration: **(a)** milliQ water and **(b)** 1 mM, **(c)** 10 mM, and **(d)** 100 mM K_2SO_4. Measurements were performed from low to high concentrations using the same cantilever.
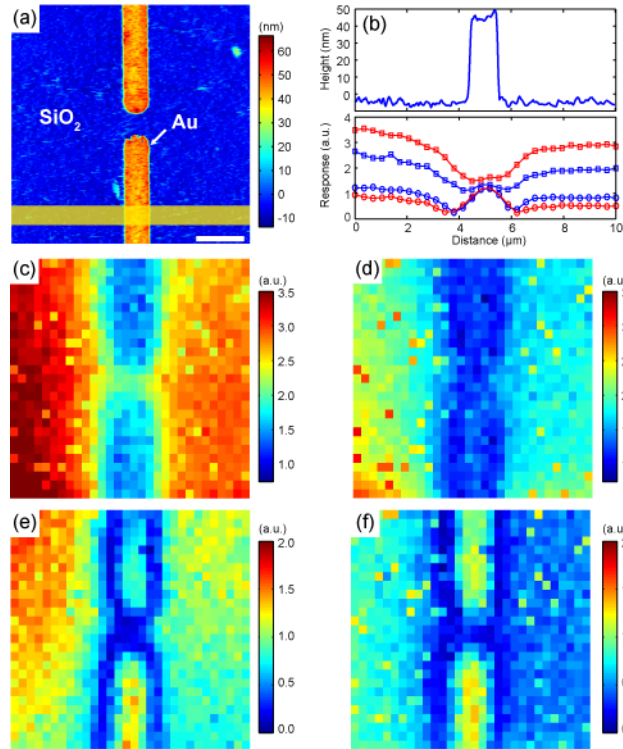
Figure 5 | Spatial variability of EcFM data recorded across Au/SiO$_2$ boundaries in milliQ water. (a) Topography image of Au electrodes on a SiO$_2$ substrate recorded using amplitude modulation AFM (scale bar = 2 μm, image size = 10 × 10 μm). (b) Average cross sectional EcFM data recorded 200 nm above the surface and determined from the area marked with a yellow box in (a) for first (squares) and second (circles) harmonic EcFM amplitude response during the application of +1.5 V (red) and -1.5 V (blue) bias pulses. Spatial variability maps from a grid of 30 × 30 2D EcFM measurements of the (c,d) first and (e,f) second harmonic EcFM amplitude response at 5 ms after the onset of the bias-on state for (c,e) +1.5 V and (d,f) -1.5 V, respectively.

References

[1] Mansfeld, F. Use of electrochemical impedance spectroscopy for the study of corrosion protection by polymer coatings. *J. Appl. Electrochem* **25**, 187-202 (1995).

[2] Böhni, H., Suter, T. & Schreyer, A. Micro-and nanotechniques to study localized corrosion. *Electrochim. Acta* **40**, 1361-1368 (1995).

[3] Drummond, T. G., Hill, M. G. & Barton, J. K. Electrochemical DNA sensors. *Nat. Biotechnol.* **21**, 1192-1199 (2003).

[4] Aricò, A.S., Bruce, P., Scrosati, B., Tarascon, J. M. & Van Schalkwijk, W. Nanostructuredmaterials for advanced energy conversion and storage devices. *Nature Mater.* **4**, 366-377 (2005).

[5] Pumera, M. Graphene-based nanomaterials for energy storage. *Energy Environ. Sci.* **4**, 668-674 (2010).

[6] Hill, H. The development of bioelectrochemistry. *Coord. Chem. Rev.* **151**, 115-123 (1996).

[7] Poizot, P., Laruelle, S., Grugeon, S., Dupont, L. & Tarascon, J. Nano-sized transition-metal oxides as negative-electrode materials for lithium-ion batteries. *Nature* **407**, 496-499 (2000).

[8] Kötz, R. & Carlen, M. Principles and applications of electrochemical capacitors. *Electrochim. Acta* **45**, 2483-2498 (2000).

[9] Carrette, L., Friedrich, K. & Stimming, U. Fuel cells–fundamentals and applications. *Fuel cells* **1**, 5-39 (2001).

[10] Bazant, M. Z., Thornton, K. & Ajdari, A. Diffuse-charge dynamics in electrochemical systems. *Phys. Rev. E* **70**, 021506 (2004).

[11] Squires, T. M. & Bazant, M. Z. Induced-charge electro-osmosis. *J. Fluid Mech.* **509**, 72-80 (2004).

[12] Bazant, M. Z., Kilic, M. S., Storey, B. D. & Ajdari, A. Towards an understanding of induced-charge electrokinetics at large applied voltages in concentrated solutions. *Adv. Colloid Interface Sci.* **152**, 48-88 (2009).

[13] Bazant, M. Z., Kilic, M. S., Storey, B. D. & Ajdari, A. Nonlinear electrokinetics at large voltages. *New J. Phys.* **11**, 075016 (2009).

[14] Nonnenmacher, M., O'boyle, M. P. & Wickramasinghe, H. K. Kelvin probe force microscopy. *Appl. Phys. Lett.* **58**, 2921-2923 (1991).

[15] Sinensky, A. K. & Belcher, A. M. Label-free and high-resolution protein/DNA nanoarray analysis using Kelvin probe force microscopy. *Nat*. *Nanotech*. **2**, 653-659 (2007).

[16] Mohn, F., Gross, L. & Meyer, G. Imaging the charge distribution within a single molecule. *Nat*. *Nanotech*. **7**, 227-231 (2012)

[17] Bazant, M. Z., & Squires T.M. Induced-charge electrokinetic phenomena: theory and microfluidic applications. *Phys. Rev. Lett.* **92,** 066101 (2004).

[18] Hillier, A. C., Kim, S. & Bard, A. J. Measurement of double-layer forces at the electrode/electrolyte interface using the atomic force microscope: potential and anion dependent interactions. *J. Phys. Chem*. **100**, 18808-18817 (1996).

[19] Raiteri, R. & Butt, H. J. Measuring electrochemically induced surface stress with an atomic force microscope. *J. Phys. Chem*. **99**, 15728-15732 (1995).

[20] Domanski, A. L. *et al.* Kelvin probe force microscopy in non-polar liquids. *Langmuir* **28**, 13892 (2012).

[21] Kobayashi, N., Asakawa, H. & Fukuma, T. Nanoscale potential measurements in liquid by frequency modulation atomic force microscopy. *Rev. Sci. Instrum.* **81**, 123705 (2010).

[22] Kobayashi, N., Asakawa, H. & Fukuma, T. Quantitative potential measurements of nanoparticles with different surface charges in liquid by open-loop electric potential microscopy. *J. Appl. Phys.* **110**, 044315 (2011).

[23] Sounart, T. L., *et al*. Frequency dependent electrostatic actuation in microfluidic MEMS. *J. Microelectromech. Syst.* **14**, 125-133 (2005).

[24] Umeda, K. *et al*. High-resolution frequency-modulation atomic force microscopy in liquids using electrostatic excitation method. *Appl. Phys. Expr.* **3**, 5205-5208 (2010).

[25] Umeda, K., Kobayashi, K., Matsushige, K. & Yamada, H. Direct actuation of cantilever in aqueous solutions by electrostatic force using high-frequency electric fields. *Appl. Phys. Lett.* **101**, 123112 (2012).

[26] Marchand, D. J., *et al*. Non-contact AFM imaging in water using electrically driven cantilever vibration. *Langmuir*, **29**, 6762-6769 (2013).

[27] Gramse, G., *et al*. Dynamic electrostatic force microscopy in liquid media. *Appl. Phys. Lett.* **101**, 213108 (2012).

[28] Gramse, G., *et al*. Nanoscale measurement of the dielectric constant of supported lipid bilayers in aqueous solutions with electrostatic force microscopy. *Biophys. J.*, **104**, 1257-1262 (2013).

[29] Umeda, K., *et al*. Analysis of capacitive force acting on a cantilever tip at solid/liquid interfaces. *J. Appl. Phys.* **113**, 154311 (2013).

[30] Kilic, M.S., Bazant M.Z., and Ajdari A. Steric effects in the dynamics of electrolytes at large applied voltages. I. Double-layer charging. *Phys. Rev. E* **75**, 021502 (2007).

[31] Kilic, M.S., Bazant M.Z., and Ajdari A. Steric effects in the dynamics of electrolytes at large applied voltages. II. Modified Poisson-Nernst-Planck equations. *Phys. Rev. E* **75**, 021503 (2007).

[32] Collins, L., *et al*. Dual harmonic Kelvin probe force microscopy at the graphene-liquid interface. *Appl. Phys. Lett.* **104**, 133103 (2014).

[33] Wang, J. *Analytical Electrochemistry*. Wiley, 2006.

[34] Collins, L., *et al*. Open loop Kelvin probe force microscopy with single and multi-frequency excitation. *Nanotechnology* **24**, 475702 (2013).

[35] Giridharagopal, R. *et al*. Submicrosecond time resolution atomic force microscopy for probing nanoscale dynamics. *Nano. Lett.* **12**, 893-898 (2012).

[36] Jolliffe, I.T. Principal Component Analysis. Springer, New York (1986).